Atmos. Chem. Phys. Discuss., https://doi.org/10.5194/acp-2017-548
Manuscript under review for journal Atmos. Chem. Phys.
Discussion started: 26 July 2017

Atmospheric Chemistry and Physics Discussions

A water vapor modulated aerosol impact on ice crystal size

Bin Zhao[1], Kuo-Nan Liou[1], Yu Gu[1], Jonathan H. Jiang[2], Qinbin Li[1], Rong Fu[1], Lei Huang[1,2], Xiaohong Liu[3], Xiangjun Shi[3], Hui Su[2], and Cenlin He[1]

[1] Joint Institute for Regional Earth System Science and Engineering and Department of Atmospheric and Oceanic Sciences, University of California, Los Angeles, California 90095, USA.

[2] Jet propulsion Laboratory, California Institute of Technology, Pasadena, California 91109, USA.

[3] Department of Atmospheric Science, University of Wyoming, Laramie, Wyoming 82071, USA.

Correspondence to: Bin Zhao (zhaob1206@ucla.edu)

Abstract.

The interactions between aerosols and ice clouds represent one of the largest uncertainties in global radiative forcing from pre-industrial time to the present. In particular, the impact of aerosols on ice crystal effective radius (R_{ei}), which is a key parameter determining ice clouds' net radiative effect, is highly uncertain due to limited and conflicting observational evidence. Here we investigate the effects of aerosols on R_{ei} under different meteorological conditions using 9-year satellite observations. We find that the responses of R_{ei} to aerosol loadings are modulated by water vapor amount in conjunction with several other meteorological parameters. While there is a significant negative correlation between R_{ei} and aerosol loading in moist conditions, consistent with the "Twomey effect" for liquid clouds, a strong positive correlation between the two occurs in dry conditions. Simulations based on a cloud parcel model suggest that water vapor modulates the relative importance of different ice nucleation modes, leading to the opposite aerosol impacts between moist and dry conditions. When ice clouds are decomposed into those generated from deep convection and formed in-situ, the water vapor modulation remains in effect for both ice cloud types, although the sensitivities of R_{ei} to aerosols differ noticeably between them due to distinct formation mechanisms. The water vapor modulation can largely explain the difference in the responses of R_{ei} to aerosol

Atmos. Chem. Phys. Discuss., https://doi.org/10.5194/acp-2017-548
Manuscript under review for journal Atmos. Chem. Phys.
Discussion started: 26 July 2017

loadings in various seasons. A proper representation of the water vapor modulation is essential for an accurate estimate of aerosol-cloud radiative forcing produced by ice clouds.

1 Introduction

Aerosols are known to interact with clouds and hence affect Earth's radiative balance, which represents the largest uncertainty in global radiative forcing from pre-industrial time to the present (IPCC, 2013). The interactions between aerosols and liquid as well as mixed-phase clouds have been extensively studied (Rosenfeld et al., 2014; Seinfeld et al., 2016), however, much less attention has been paid to ice clouds, among which cirrus clouds are globally distributed and present at all latitudes and seasons with a global cloud cover of about 30% (Wylie et al., 1994; Wylie et al., 2005). Ice clouds, formed with various types of aerosols serving as ice nucleating particles (INPs) (Murray et al., 2012; Hoose and Moehler, 2012), act as a major modulator of global radiation budget and hence climatic parameters (e.g., temperature and precipitation) by reflecting solar radiation back to space (solar albedo effect, cooling) and by absorbing and re-emitting long-wave terrestrial radiation (greenhouse effect, warming); the balance between the two is dependent on ice cloud properties, particularly ice crystal size (Liou, 2005; Waliser et al., 2009; Fu and Liou, 1993). Limited estimates (IPCC, 2013; Liu et al., 2009; Fan et al., 2016) have shown that the global aerosol-cloud radiative forcing produced by ice clouds can be very significant but highly uncertain, ranging from –0.67 W m^{-2} to 0.70 W m^{-2}. For reference purposes, the best estimate of global aerosol-cloud radiative forcing produced by all cloud types is –0.45 W m^{-2} (90% confidence interval [–1.2, 0 W/m^2]) according to the Intergovernmental Panel on Climate Change (IPCC) (Fig. TS.6 in IPCC, 2013).

The substantial uncertainty in aerosol-ice cloud radiative forcing arises largely from a poor understanding of the aerosol effects on ice cloud properties, in particular ice crystal effective radius (R_{ei}), a key parameter determining ice clouds' net radiative effect (Fu and Liou, 1993). Very limited observational studies (Jiang et al., 2008; Jiang et al., 2011; Su et al., 2011; Chylek et al., 2006; Massie et al., 2007) have investigated the response of R_{ei} to aerosol loadings. Most of them (Jiang et al., 2008; Jiang et al., 2011; Su et al., 2011) found that polluted clouds involved smaller R_{ei} than clean clouds, in agreement with the classical "Twomey effect" for liquid clouds (Twomey, 1977), which states that more aerosols can result in more and smaller cloud droplets and hence larger cloud albedo. In contrast, a couple of studies over the Indian Ocean (Chylek et al., 2006; Massie et al., 2007) reported that R_{ei} is

Atmos. Chem. Phys. Discuss., https://doi.org/10.5194/acp-2017-548
Manuscript under review for journal Atmos. Chem. Phys.
Discussion started: 26 July 2017

roughly unchanged (Massie et al., 2007) or larger (Chylek et al., 2006) during more polluted episodes. It has been shown that increased aerosols (and thus INPs) lead to enhanced heterogeneous nucleation, which is associated with larger and fewer ice crystals as compared to the homogeneous nucleation counterpart (DeMott et al., 2010; Chylek et al., 2006). However, the reasons for disagreement among various studies, and the controlling factors for different aerosol indirect effects are yet to be explored, therefore the sign and magnitude of the overall aerosol effects remain in question.

With the objective to resolve the substantial uncertainty, we systematically investigate the effects of aerosols on R_{ei} of two types of ice clouds under different meteorological conditions using 9-year continuous satellite observations from 2007 to 2015. The study region is East Asia and its surrounding areas (15º-55º N, 70º-135º E; Fig. S1), where aerosol loadings can range from small to extremely large values in different locations and time periods (Wang et al., 2017).

2 Data and Methods

2.1 Sources of observational data

We obtain collocated aerosol/cloud measurements primarily from MODIS (Moderate Resolution Imaging Spectroradiometer) onboard the Aqua satellite, and CALIPSO (Cloud-Aerosol Lidar and Infrared Pathfinder Satellite Observations), as summarized in Table S1.

We acquire aerosol optical depth (AOD) retrievals at 550 nm from the level 2 MODIS aerosol product (MYD04, Collection 6) at a resolution of 10 km × 10 km. The accuracy of AOD (denoted by τ) retrievals has been estimated to be about $\pm(0.05 + 0.15\tau)$ over land and $\pm(0.03 + 0.05\tau)$ over ocean (Levy et al., 2010; Remer et al., 2005). Similarly, we obtain cloud effective radius (equivalent to R_{ei} in the case of ice phase) and cloud phase determined by the "cloud optical property" algorithm from the level 2 MODIS cloud product (MYD06, Collection 6) at a 1 km × 1 km resolution (Platnick et al., 2015).

The CALIPSO satellite flies behind Aqua by about 75 seconds and carries CALIOP (Cloud-Aerosol Lidar with Orthogonal Polarization), a dual-wavelength near-nadir polarization lidar (Winker et al., 2007). CALIOP has the capability to determine the global vertical distribution of aerosols and clouds. In this study, we make use of the CALIPSO level 2 merged aerosol and cloud layer product (05kmMLay, version 4.10) with an along-track resolution of 5 km and a high vertical resolution of 30-60 m below 20.2 km. The variables we employ for the investigation include aerosol/cloud layer numbers, layer base temperature,

Atmos. Chem. Phys. Discuss., https://doi.org/10.5194/acp-2017-548
Manuscript under review for journal Atmos. Chem. Phys.
Discussion started: 26 July 2017

layer top/base height, layer aerosol/cloud optical depth, feature classification flags (containing the flags of "cloud type" and "aerosol type"), and two quality control (QC) flags named the cloud aerosol discrimination (CAD) score, and extinction QC (Atmospheric Science Data Center, 2012).

To examine the impact of meteorological conditions on aerosol-R_{ei} relations, we also obtain vertically-resolved pressure, relative humidity (RH), and temperature from the CALIPSO aerosol profile product (05kmAPro, version 4.10), and middle cloud layer temperature (T_{mid}) from the CALIPSO 05kmMLay product (version 4.10). The other meteorological parameters (see Table S1) are collected from the NCEP's Final Analysis reanalysis data (ds083.2), which are produced at a 1° × 1° resolution every six hours. Since Aqua and CALIPSO satellites overpass the study areas between 5:00-8:00 UTC, the ds083.2 datasets at 6:00 UTC are utilized.

2.2 Processing of observational data

In the analysis, we identify a CALIPSO profile layer at 5 km resolution as ice cloud when its "cloud type" is "cirrus" or its layer base temperature is colder than –35 °C. Previous studies (Mace et al., 2001; Mace et al., 2006; Kramer et al., 2016) have distinguished two major types of ice clouds characterized by distinct formation mechanisms: ice clouds generated from deep convection (convective ice clouds) and those generated in-situ due to updraft caused by frontal systems, gravity waves, or orographic waves (in-situ ice clouds). Considering that the impact of aerosols could be discrepant in different formation processes, we separate these two ice cloud types using CALIPSO data and a similar approach to that developed by Riihimaki and McFarlane (2010). First, we group ice cloud profiles at 5 km resolution into objects using the criteria that neighboring ice cloud profiles must vertically overlap (the base of the higher cloud layer is lower than the top of the lower cloud layer) and be separated by no more than 1 profiles horizontally (i.e., distance $\leqslant$ 5 km). We subsequently classify ice cloud objects into three types, i.e., convective, in-situ, and other ice clouds, according to their connection to other clouds. The criteria to determine whether two clouds are connected are consistent with that used to group ice cloud objects, i.e., the neighboring profiles must vertically overlap and horizontally seperated by no more than 5 km. Convective ice clouds consist of ice cloud objects that are connected to larger clouds that include deep convective profiles (i.e., the "cloud type" flag is "deep convection"). An ice cloud object is classified as in-situ if at least 95% of a cloud consists of a single ice cloud object which is at least 25 km (i.e., 5 profiles) in

the horizontal direction, and none of the remaining profiles are deep convection type. The remaining ice cloud objects are catogorized as the "other" type. The convective, in-situ, and other ice clouds account for 44.9%, 52.4%, and 2.7% of all ice cloud profiles, respectively. The "other" type is neglected in the subsequent analysis due to very small occurrence frequency. We should be cautious that the convective and in-situ ice clouds may not be perfectly separated using the approach described above. For example, the in-situ ice clouds indentified here could include convectively-detrained objects that are no longer connected with their parent deep convection, and convectively-detrained objects whose parent deep convective clouds do not overlap with CALIPSO's track. The convective ice clouds may also be contaminated by some in-situ formed ice cloud objects that happen to be spatially connected to deep convection. However, the classification scheme appears to be reasonable, as indicated by the distinct properties of the two ice cloud types shown in Section 3.2. Only single-layer ice cloud profiles with valid QA flags (20 $\leqslant$ CAD score $\leqslant$ 100, Extinction QC = 0/1) are used in statistical analysis.

We then match collocated MODIS/Aqua and CALIPSO observations by averaging retrieved AOD and R_{ei} from MODIS level 2 products (MYD04 and MYD06) within 30 km and 5 km radii of each 5 km ice cloud profile from CALIPSO, respectively. The averaging is done to achieve near-simultaneous aerosol and cloud measurements, since AOD observations from MODIS are missing at cloudy conditions. As AOD variation has a large spatial length scale of 40-400 km (Anderson et al., 2003), it is averaged within a larger radius than that for R_{ei} to increase the number of data points with valid AOD observations. The average R_{ei} is calculated based on the pixels with "cloud phase" of ice. Apart from the column AOD, we also need to obtain AOD of the aerosol layers mixed with ice cloud layers, as in-situ ice clouds are primarily affected by aerosols at the ice cloud height. For this purpose, we use the CALIPSO 05kmMLay product to select the aerosol layers which have valid QA flags (-100 $\leqslant$ CAD score $\leqslant$ -20, Extinction QC = 0/1; Huang et al., 2013) and are vertically less than 0.25 km away from the ice cloud layer following Costantino and Breon (2010). The AOD of these aerosol layers are averaged within a 30 km radius of ice cloud profiles. The meteorological parameters from the NCEP datasets (ds083.2) are matched to the CALIPSO resolution by determining which NCEP's grid contains a certain CALIPSO 5 km profile. Finally, we eliminate profiles with column AOD > 1.5 to reduce the potential effect of cloud contamination (Wang et al., 2015).

Convective ice clouds are generated by convective updraft originating from lower troposphere and are therefore affected by aerosols at various altitudes, whereas in-situ ice clouds are primarily dependent on aerosols near the cloud height. For this reason, we use column AOD and layer AOD mixed with ice clouds as proxies for aerosols interacting with convective and in-situ ice clouds, respectively. We also investigate the overall effect of aerosols on all types of ice clouds. In this case, column AOD is used as a proxy for aerosol loading affecting ice clouds following a number of previous studies (Jiang et al., 2011; Massie et al., 2007; Ou et al., 2009). The rationale is that the MODIS-detected AOD generally shows a close correlation to the MLS (Microwave Limb Sounder)-observed CO concentration in ice clouds (Jiang et al., 2008; Jiang et al., 2009), which in turn correlates well with the aerosol loading mixed with clouds in accordance with both aircraft measurements and atmospheric modeling (Jiang et al., 2009; Li et al., 2005; Clarke and Kapustin, 2010). After the preceding screening, about 2.73×10^4, 1.09×10^4, and 5.68×10^4 profiles are used to analyze the relationships between column/layer AOD and R_{ei} of convective, in-situ, and all types of ice clouds. The available profiles for in-situ ice clouds are fewer because aerosols mixed with ice clouds are often optically thin or masked by clouds and hence may not be fully detected by CALIPSO.

2.3 Cloud parcel model simulation

To support the key findings (i.e., the water vapor modulation of R_{ei}-aerosol relations) from satellite observations and elucidate the underlying physical mechanisms, we perform model simulations using a cloud parcel model, which was originally developed by Shi and Liu (2016) and updated in this study to incorporate immersion nucleation. The model mimics formation and evolution of in-situ ice clouds in an adiabatically rising air parcel. The formation of convective ice clouds involves additional physical processes, which call for more sophisticated models and future investigations. Nevertheless, as will be discussed in Section 3.4, the key processes controlling the patterns of R_{ei}-aerosol relations should be similar for these two ice cloud types. The model's governing equations that describe the evolution of temperature, pressure, and mass mixing ratio, number concentration, and size of ice crystals can be found in Pruppacher and Klett (1997). The main microphysical processes considered include homogeneous nucleation and two modes of heterogeneous nucleation (deposition and immersion nucleation), depositional growth, sublimation, and sedimentation. The rate of homogeneous nucleation of supercooled sulfate droplets is calculated based on the water activity of sulfate solution (Shi and Liu, 2016). The dry sulfate aerosol is assumed to follow a

lognormal size distribution with a geometric mean radius of 0.02 μm. The deposition nucleation on externally mixed dust (deposition INP) and immersion nucleation of coated dust (immersion INP) are parameterized following Kuebbeler et al. (2014). Anthropogenic INPs are not included in the cloud parcel model following recent studies (Shi and Liu, 2016; Kuebbeler et al., 2014). This is because 1) ice nucleation experiments for black carbon show contradicting results (Hoose and Moehler, 2012), and 2) ice nucleation parameterizations for anthropogenic aerosol constituents other than black carbon have not been adequately developed under ice cloud conditions due to limited experimental data. Also, we find that the relationships between R_{ei} and loadings of dust aerosols are similar to those between R_{ei} and loadings of all aerosols (Section 3.1). As such, we argue that the general pattern of simulation results would remain unchanged if more INPs were incorporated. The accommodation coefficient of water vapor deposition on ice crystals is assumed to be 0.1 (Shi and Liu, 2016). The sedimentation velocity of ice crystals is parameterized following Ikawa and Saito (1991). The model neglects some ice microphysical processes such as aggregational growth of ice crystals. Although aggregational growth can affect the concentration and size of ice crystals, its effects should be relatively small in terms of the response of R_{ei} to aerosol loading since this process is not strongly dependent on aerosols.

We conduct three groups of numerical experiments with discrepant available water amount for ice formation, denoted by initial water vapor mass mixing ratios (pv). Each group is comprised of 100 experiments with initial sulfate number concentrations increasing linearly from 5 cm^{-3} to 500 cm^{-3}. For all experiments, the initial number concentrations of externally mixed dust and coated dust are prescribed to be 0.015% and 0.005% of sulfate, respectively, since INPs represent only 1 in 10^3 to 10^6 of ambient particles (Fan et al., 2016). The initial pressure and temperature for all experiments are set at 250 hPa and 220 K, respectively. The updraft velocity is prescribed to be 0.5 m s^{-1} along with the simulation period which covers a length of 30 min. The effective radius, number concentration, and mass mixing ratio of ice crystals at the end of the experiments are used to construct the aerosol-cloud relationships.

3 Results and Discussion

3.1 Relationships between R_{ei} and aerosols modulated by meteorology

In this section we discuss the impact of aerosols on R_{ei}, with both ice cloud types lumped together, based on satellite data (Fig. 1). The aerosol effects on individual ice cloud types will be discussed in the next section. The dash line in Fig. 1a shows the overall changes in R_{ei} with

Atmos. Chem. Phys. Discuss., https://doi.org/10.5194/acp-2017-548
Manuscript under review for journal Atmos. Chem. Phys.
Discussion started: 26 July 2017

AOD. R_{ei} generally increases with increasing AOD for moderate AOD range (< 0.5), and decreases slightly for higher AOD. This relationship is attributable to complex interactions between meteorological conditions and microphysical processes, which will be detailed below.

Having shown overall response of R_{ei} to AOD, we investigate whether the responses are similar under different meteorological conditions. We plot the R_{ei}-AOD relationships separately for different ranges of meteorological parameters, as shown in Fig. 1a-c and Fig. S2. Included in the analysis are most meteorological parameters that can potentially affect ice cloud formation and evolution, including the RH averaged between 100 hPa and 440 hPa, convective available potential energy (CAPE) which is an indicator of convective strength, middle cloud layer temperature (T_{mid}), wind speed and direction at ice cloud height and at surface, vertical velocity below and at ice cloud height, and vertical wind shear. For some meteorological parameters, e.g., vertical wind shear and vertical velocity at 300/500 hPa, the curve shapes are similar for different meteorological ranges. However, for RH, CAPE, and U-component of wind speed at 200 hPa (U200), the curve shapes vary significantly according to different ranges (Fig. 1a-c). As illustrated by RH and CAPE, R_{ei} decreases significantly with increasing AOD for high RH (> 65%) or CAPE (> 500 J/kg) following the rule of "Twomey effect". In contrast, for low RH (< 45%) or CAPE (0 J/kg), R_{ei} increases sharply with AOD. To the best of our knowledge, the strong dependency of R_{ei}-AOD relationships on meteorological conditions for ice clouds has been demonstrated for the first time.

These correlations, however, may not be necessarily attributed to aerosols. It is theoretically possible that certain meteorological parameters lead to simultaneous changes in both AOD and ice cloud properties and produce a correlation between these two parameters. To rule out this possibility, we examine the responses of AOD to the above-mentioned meteorological parameters (Fig. S3) and find that AOD does not serve as proxy for them since it varies by less than 0.2 in response to variation in any meteorological parameter. Furthermore, we bin observed R_{ei} according to RH, CAPE, and U200, for different ranges of AOD (Fig. 1d-f). Using RH as an example, a larger AOD corresponds to smaller R_{ei} for a given RH within the larger RH range, whereas an increase in AOD enlarges R_{ei} for a given RH within the smaller RH range. Similar results are found for CAPE and U200 (Fig. 1d-f), demonstrating the role of aerosols in altering R_{ei} under the same meteorological conditions. Moreover, the cloud contamination in AOD retrieval (Kaufman et al., 2005) or aerosol contamination in cloud retrieval (Brennan et al., 2005) is not likely to lead to observed R_{ei}-AOD correlations, because the retrieval biases cannot explain the opposite correlations under

different meteorological conditions. Therefore, we conclude that both the positive and negative correlations between AOD and R_{ei} are primarily attributed to the aerosol effect. This causality is also supported by numerical simulations using a cloud parcel model to be described in Section 3.4. Furthermore, we find that the three meteorological parameters which pose the strongest impact on R_{ei}-AOD relationships (RH, CAPE, and U200) are closely correlated with each other, with correlation coefficients between each two exceeding ±0.5 and p-value less than 0.01 (Table S2). In fact, all these three parameters are closely related to the amount of water vapor available for ice cloud formation. It is obvious that RH averaged between 100-440 hPa is an indicator of water vapor amount. CAPE represents convective strength and hence water vapor lifted to ice cloud heights; U200 denotes the origin of air mass such as moist Pacific Ocean (easterly wind) or dry inland continent (westerly wind). Therefore, water vapor amount is likely a key factor which modulates the observed impact of aerosols on R_{ei}.

The proposed mechanism for the water vapor modulation is that different water vapor amount substantially alters the relative significance of different ice nucleation modes, thereby resulting in discrepant R_{ei}-AOD relationships. Specifically, ice crystals form via two primary pathways: homogeneous nucleation of liquid water droplets (or supercooled solution particles) below about −35 °C, and heterogeneous nucleation triggered by INPs (IPCC, 2013; DeMott et al., 2010). INPs possess surface properties favorable to lowering the ice supersaturation ratio required for freezing (IPCC, 2013; DeMott et al., 2010), therefore the onset of heterogeneous nucleation is generally easier and earlier in rising air parcels. Under moist conditions, homogeneous nucleation dominates and thus more aerosols could lead to the formation of more and smaller ice crystals, which is in connection with the “Twomey effect” for liquid clouds. Under dry conditions, however, the earlier onset of heterogeneous nucleation can strongly compete with and possibly prevent homogeneous nucleation involving more abundant water-bearing or solution particles (IPCC, 2013; DeMott et al., 2010). Therefore, more aerosols (and hence more INPs) are expected to lead to a higher fraction of ice crystals produced by heterogeneous nucleation comprising of fewer and larger ice crystals (“anti-Twomey effect”). These proposed mechanisms will be supported and elaborated on using model simulations in Section 3.4.

Here an inherent assumption is that INP concentration is roughly proportional to, or at least positively correlated with AOD. Considering that INPs only account for a small fraction of ambient aerosols, we may not take this assumption for granted. Here we plot the R_{ei}-AOD

relations using only the cases in which the "aerosol type" (a flag contained in the feature classification flags of CALIPSO) is dust (Fig. 1g-i), and find that the water modulation effect is very similar to the preceding results (i.e., Fig. 1a-c). Since specific components of dust aerosols have been known as effective INPs (Murray et al., 2012; Hoose and Moehler, 2012), the similar R_{ei}-AOD relations of dust and of all aerosols to some extent support the proposed mechanisms for water vapor modulation.

3.2 R_{ei}-aerosol relationships for two types of ice clouds

Considering that distinct formation mechanisms of convective and in-situ ice clouds may lead to different aerosol effects, we distinguish these two ice cloud types based on their connection to deep convection (Section 2.2). Figure 2 illustrates the accumulative probability distribution of cloud thickness, cloud optical thickness (COT), and R_{ei} of the two ice cloud types. The cloud thickness and COT of convective ice clouds are remarkably larger than those of in-situ ice clouds, because more water is transported to upper troposphere in the formation process of the former type, consistent with numerous aircraft measurement results (e.g., Kramer et al., 2016; Luebke et al., 2016; Muhlbauer et al., 2014). The R_{ei} of convective ice clouds is slightly larger than that of in-situ ice clouds, which has also been reported in a number of aircraft campaigns (Luebke et al., 2016; Kramer et al., 2016). The larger R_{ei} in convective ice clouds is attributed to larger water amount and the fact that they are produced by convection emerging from lower altitude. Below the –35 ^{o}C isotherm, ice crystals stem only from heterogeneous nucleation, which tends to produce larger ice crystals compared to the homogeneous nucleation counterpart (Luebke et al., 2016).

Figures 3 and 4 show the impact of aerosols on R_{ei} under different meteorological conditions for convective and in-situ ice clouds, respectively. As described in Section 2.2, we use column AOD and layer AOD mixed with ice clouds as proxies of aerosols interacting with convective and in-situ ice clouds, respectively. The most impressive feature from these figures is that the meteorology modulation remains in effect for either of the two ice cloud types, such that R_{ei} generally decreases with AOD under high RH/high CAPE/negative U200 conditions, whereas the reverse is true under low RH/low CAPE/positive U200 conditions. Similar to the Section 3.1, we also demonstrate that the R_{ei}-aerosol relationships are primarily attributed to the aerosol effect by illustrating role of aerosols in altering R_{ei} under the nearly constant meteorological conditions (Fig. 3d-f, Fig. 4d-f). For example, a larger AOD is associated with a smaller R_{ei} for a given RH within the larger RH range, while an increase in AOD leads to a larger R_{ei} for a given RH within the smaller RH range. These results illustrate

Atmos. Chem. Phys. Discuss., https://doi.org/10.5194/acp-2017-548
Manuscript under review for journal Atmos. Chem. Phys.
Discussion started: 26 July 2017

that the meterology modulation of aerosol effects on R_{ei} is valid regardless of ice cloud formation machanisms.

A closer look at Figs. 3 and 4 shows that there exist noted differences between the R_{ei}-aerosol relationships for the two ice cloud types. For convective ice clouds, a strong positive correlation between R_{ei} and AOD is found under dry conditions, while a weaker negative correlation is found under moist conditions. For in-situ ice clouds, however, weaker positive and stronger negative correlations are shown under dry and moist conditions, respectively. As a result, overall R_{ei} slightly increases with increasing aerosol loading for convective ice clouds, but slightly dcreases for in-situ clouds. These differences are again linked to the distinct formation mechanisms of the two ice cloud types. Convective ice clouds are influenced by aerosols at various heights, which presumably contain much more INPs than the thin upper tropospheric aerosol layers in the case of in-situ ice clouds. In addition, the heterogeneously formed ice crystals in convective clouds are able to grow before being lifted to the –35 ^{o}C isotherm, giving rise to a larger difference between the ice crystal sizes produced by heterogeneous and homogeneous nucleation as compared to in-situ ice clouds. For these reasons, under dry conditions, the increase in R_{ei} with aerosol loading, which is due to the transition from homogeneous-dominated to heterogeneous-dominated regimes, would be much more pronounced for convective ice clouds. At moist conditions, although homogeneous nucleation dominates for both ice cloud types (see Section 3.1), the mass fraction of homogeneously formed ice crystals is smaller for convective ice clouds, leading to a weaker decline in R_{ei} with aerosols.

3.3 Seasonal variations in R_{ei}-aerosol relationships

Furthermore, we find that the meteorological modulation can largely explain differences in R_{ei}-AOD relationships as a function of season. Figure 5a shows that the R_{ei}-AOD relationships are dramatically different associated with season, such that R_{ei} decreases significantly with increasing AOD in summer (June, July, and August), while R_{ei} increases rapidly in winter (December, January, and February). Figure 5d-f illustrate the probability distribution functions (PDFs) of RH, CAPE, and U200 in different seasons (the area under any PDF equals 1.0). The overlapping area of PDFs in summer and winter represents the degree of difference in meteorological conditions between these two seasons. We find that meteorological conditions are significantly distinct in summer and winter in terms of RH, CAPE, and U200, as indicated by relatively small overlapping areas (<0.6) for these three parameters. The RH and CAPE tend to be higher and U200 tends to be more negative in

summer. Moreover, the shapes of R_{ei}-AOD curves in summer and winter highly resemble those under high-RH/high-CAPE/negative-U200 and low-RH/low-CAPE/positive-U200 conditions, respectively (see Fig. 1a-c), which demonstrates that the discrepancy in meteorological conditions between winter and summer can, to a large extent, explain the distinct R_{ei}-AOD relationships in these two seasons. Furthermore, when ice clouds are decomposed into convective and in-situ types, Fig. 5b-c show that the above-mentioned patterns hold true for both types, indicating that the seasonal variations in R_{ei}-aerosol relations for both ice cloud types are largely attributable to the meteorology modulation.

3.4 Modeling support for the water vapor modulation

We have shown that the R_{ei}-aerosol relationships are modulated by meteorological conditions, particularly water vapor amount. To support the observed relationships and our proposed physical mechanisms, we perform model simulations as described in Section 2.3 and summarize the results in Fig. 6.

Figure. 6a reveals that the simulated patterns of R_{ei}-aerosol relationships under different water vapor amount agree well with the corresponding observed patterns (Fig. 1a-c). Specifically, with adequate water vapor (pv = 106 ppm), R_{ei} decreases significantly with aerosol concentrations ("Twomey effect"). Under a dry condition (pv = 38 ppm), R_{ei} increases noticeably with aerosol concentrations ("anti-Twomey effect"). With a medium water vapor amount (pv = 53 ppm), R_{ei} first decreases and then increases. A deeper analysis of the simulation results supports our proposed mechanism (Section 3.1) that the competition between different ice nucleation modes is the key to explain the water vapor modulation. With adequate water vapor (pv = 106 ppm), the onset of deposition and immersion nucleation under relatively lower ice supersaturation consumes only a small fraction of water vapor due to the small INP population, and homogeneous nucleation acts as the dominant ice formation pathway, as indicated by the very small number/mass fraction (< 1%) of heterogeneously formed ice crystals shown in Fig. 6b. In this case, more aerosols are associated with the formation of more and smaller more and smaller ice crystals, consistent with the simulation results of Liu and Penner (2005). With inadequate water vapor (pv = 38 ppm), Fig. 6b reveals that the number fraction of heterogeneously formed ice crystals increases dramatically from about 30% to nearly 100% when aerosol number concentrations increase from 5 cm^{-3} to ~300 cm^{-3} (the INP number concentrations increase proportionally). This indicates that the water vapor consumed by heterogeneous nucleation is large enough to suppress or even prevent homogeneous nucleation that occurs spontaneously over a higher and narrow ice

supersaturation range (140-160%). Since the outburst of homogeneous nucleation generally produces more ice crystals at smaller size compared with the heterogeneous counterpart, an increasing fraction of heterogeneous nucleation would result in fewer ice crystals with larger average size.

The current cloud parcel model simulates the environmental conditions and physical processes for in-situ ice clouds. Although the formation processes of convective ice clouds are considerably different from those of in-situ ones, the competition between homogeneous and heterogeneous nucleation for water vapor hold true for both ice cloud types, and is very likely to explain the water vapor modulation of R_{ei}-aerosol relations for both types. Nevertheless, more simulation studies are still needed to support and better understand the discrepant sensitivities of R_{ei} to aerosols for these two cloud types.

As a simplified model, the simulation results of the cloud parcel model may not be directly compard with the satellite observations. For example, we use column/layer AOD and RH averaged between 100-440 hPa (and CAPE, U200) as proxies for aerosol loading and available water amount, repectively, in satellite data analysis. In contrast, the concentrations of aerosols and water vapor within a single air parcel are employed in the model simulation. A direct comparison between satellite observations and model simulations would require running a 3-D atmospheric model, which calls for further in-depth studies. It is also noted that the model-simulated magnitude of R_{ei} is generally smaller than observations probably due to limited simulation periods, exclusion of ice aggregational growth and water vapor uptake from outside of the air parcel, and variability in updraft velocity (Kramer et al., 2016; Feingold, 2003); nevertheless, the model has successfully reproduced the key microphysical processes and hence captured the observed patterns of R_{ei}-aerosol relationships.

4 Conclusions and implications

In this study, we investigate the effects of aerosols on R_{ei} under different meteorological conditions using 9-year satellite observations. We find that the responses of R_{ei} to aerosol loadings are modulated by water vapor amount in conjunction with several other meteorological parameters, and vary from a significant negative correlation ("Twomey effect") to a strong positive correlation ("anti-Twomey effect"). Simulations using a cloud parcel model indicate that the water vapor modulation works primarily by altering the relative importance of different ice nucleation modes. The water vapor modulation holds true for both convective and in-situ ice clouds, though the sensitivities of R_{ei} to aerosols differ noticeably between these two ice cloud types due to distinct formation mechanisms. The water vapor

modulation can largely explain the different responses of R_{ei} to aerosol loadings in various seasons.

R_{ei} is a key parameter determining the relative significance of the solar albedo (cooling) effect and the infrared greenhouse (warming) effect of ice clouds; the variation of R_{ei} could change the sign of ice clouds' net radiative effect (Fu and Liou, 1993). Aerosols have strong and intricate effects on R_{ei} through their indirect effect. We provide the first and direct evidence that the competition between the "Twomey effect" and "anti-Twomey effect" is controlled by certain meteorological parameters, primarily water vapor amount. Consequently, the first aerosol indirect forcing, defined as the radiative forcing due to aerosol-induced changes in R_{ei} under a constant ice water content (IPCC, 2013; Penner et al., 2011), would change from positive to negative between high and low RH ranges, implying that the water vapor modulation could play an important role in determining the sign, magnitude, and probably seasonal and regional variations of aerosol-ice cloud radiative forcings. An adequate and accurate representation of this modulation in climate models will undoubtedly induce changes in the magnitude and sign of the current estimate of aerosol-ice cloud radiative forcing. Finally, although this study focuses on East Asia, we anticipate that the present findings might be generalized to other regions as well in view of the fact that the aerosol loadings in East Asia usually span a larger range than other regions and that the aerosol effects on ice cloud properties are particularly pronounced at low and moderate aerosol loadings (Figs. 1, 3, 4, 5).

Acknowledgements

Research work contained in this paper has been supported by NSF EAGER Grant AGS-1523296 and NASA ROSES ACMAP and CCST grants. We also acknowledge the support of the Joint Institute for Regional Earth System Science and Engineering at University of California, Los Angeles and the Jet Propulsion Laboratory, California Institute of Technology, under contract with NASA.

References

Anderson, T. L., Charlson, R. J., Winker, D. M., Ogren, J. A., and Holmen, K.: Mesoscale variations of tropospheric aerosols, J Atmos Sci, 60, 119-136, Doi 10.1175/1520-0469(2003)060<0119:Mvota>2.0.Co;2, 2003.

Atmospheric Science Data Center: CALIPSO Quality Statements Lidar Level 2 Cloud and Aerosol Layer Products Version Releases: 3.01, 3.02: https://eosweb.larc.nasa.gov/PRODOCS/calipso/Quality_Summaries/CALIOP_L2Layer Products_3.01.html, access: October 1, 2016, 2012.

Brennan, J. I., Kaufman, Y. J., Koren, I., and Li, R. R.: Aerosol-cloud interaction-misclassification of MODIS clouds in heavy aerosol, IEEE T Geosci Remote, 43, 911-915, 10.1109/Tgrs.2005.844662, 2005.

Chylek, P., Dubey, M. K., Lohmann, U., Ramanathan, V., Kaufman, Y. J., Lesins, G., Hudson, J., Altmann, G., and Olsen, S.: Aerosol indirect effect over the Indian Ocean, Geophys Res Lett, 33, L06806, DOI 10.1029/2005gl025397, 2006.

Clarke, A., and Kapustin, V.: Hemispheric aerosol vertical profiles: Anthropogenic impacts on optical depth and cloud nuclei (vol 329, pg 1488, 2010), Science, 330, 1047-1047, 2010.

Costantino, L., and Breon, F. M.: Analysis of aerosol-cloud interaction from multi-sensor satellite observations, Geophys Res Lett, 37, L11801, DOI 10.1029/2009gl041828, 2010.

DeMott, P. J., Prenni, A. J., Liu, X., Kreidenweis, S. M., Petters, M. D., Twohy, C. H., Richardson, M. S., Eidhammer, T., and Rogers, D. C.: Predicting global atmospheric ice nuclei distributions and their impacts on climate, P Natl Acad Sci USA, 107, 11217-11222, 10.1073/pnas.0910818107, 2010.

Fan, J. W., Wang, Y., Rosenfeld, D., and Liu, X. H.: Review of Aerosol–Cloud Interactions: Mechanisms, Significance, and Challenges, J Atmos Sci, 73, 4221-4252, 2016.

Feingold, G.: Modeling of the first indirect effect: Analysis of measurement requirements, Geophys Res Lett, 30, 10.1029/2003gl017967, 2003.

Fu, Q., and Liou, K. N.: Parameterization of the Radiative Properties of Cirrus Clouds, J Atmos Sci, 50, 2008-2025, Doi 10.1175/1520-0469(1993)050<2008:Potrpo>2.0.Co;2, 1993.

Hoose, C., and Moehler, O.: Heterogeneous ice nucleation on atmospheric aerosols: a review of results from laboratory experiments, Atmos Chem Phys, 12, 9817-9854, 10.5194/acp-12-9817-2012, 2012.

Huang, L., Jiang, J. H., Tackett, J. L., Su, H., and Fu, R.: Seasonal and diurnal variations of aerosol extinction profile and type distribution from CALIPSO 5-year observations, J Geophys Res-Atmos, 118, 4572-4596, 10.1002/jgrd.50407, 2013.

Ikawa, M., and Saito, K.: Description of a Non-hydrostatic Model Developed at the Forecast Research Department of the MRI, Meteorological Research Institute, Tsukuba, Ibaraki, Japan, 1991.

IPCC: Climate Change 2013: The Physical Science Basis. Contribution of Working Group I to the Fifth Assessment Report of the Intergovernmental Panel on Climate Change, edited by: Stocker, T. F., Qin, D., Plattner, G.-K., Tignor, M., Allen, S. K., Boschung, J., Nauels, A., Xia, Y., Bex, V., and Midgley, P. M., Cambridge University Press, Cambridge, United Kingdom and New York, NY, USA, 1535 pp., 2013.

Jiang, J. H., Su, H., Schoeberl, M. R., Massie, S. T., Colarco, P., Platnick, S., and Livesey, N. J.: Clean and polluted clouds: Relationships among pollution, ice clouds, and precipitation in South America, Geophys Res Lett, 35, L14804, DOI 10.1029/2008gl034631, 2008.

Jiang, J. H., Su, H., Massie, S. T., Colarco, P. R., Schoeberl, M. R., and Platnick, S.: Aerosol-CO relationship and aerosol effect on ice cloud particle size: Analyses from Aura Microwave Limb Sounder and Aqua Moderate Resolution Imaging Spectroradiometer observations, J Geophys Res-Atmos, 114, D20207, DOI 10.1029/2009jd012421, 2009.

Jiang, J. H., Su, H., Zhai, C., Massie, S. T., Schoeberl, M. R., Colarco, P. R., Platnick, S., Gu, Y., and Liou, K. N.: Influence of convection and aerosol pollution on ice cloud particle effective radius, Atmos Chem Phys, 11, 457-463, 10.5194/acp-11-457-2011, 2011.

Kaufman, Y. J., Koren, I., Remer, L. A., Rosenfeld, D., and Rudich, Y.: The effect of smoke, dust, and pollution aerosol on shallow cloud development over the Atlantic Ocean, P Natl Acad Sci USA, 102, 11207-11212, 10.1073/pnas.0505191102, 2005.

Kramer, M., Rolf, C., Luebke, A., Afchine, A., Spelten, N., Costa, A., Meyer, J., Zoger, M., Smith, J., Herman, R. L., Buchholz, B., Ebert, V., Baumgardner, D., Borrmann, S., Klingebiel, M., and Avallone, L.: A microphysics guide to cirrus clouds - Part 1: Cirrus types, Atmos Chem Phys, 16, 3463-3483, 10.5194/acp-16-3463-2016, 2016.

Kuebbeler, M., Lohmann, U., Hendricks, J., and Karcher, B.: Dust ice nuclei effects on cirrus clouds, Atmos Chem Phys, 14, 3027-3046, 10.5194/acp-14-3027-2014, 2014.

Levy, R. C., Remer, L. A., Kleidman, R. G., Mattoo, S., Ichoku, C., Kahn, R., and Eck, T. F.: Global evaluation of the Collection 5 MODIS dark-target aerosol products over land, Atmos Chem Phys, 10, 10399-10420, 10.5194/acp-10-10399-2010, 2010.

Li, Q. B., Jiang, J. H., Wu, D. L., Read, W. G., Livesey, N. J., Waters, J. W., Zhang, Y. S., Wang, B., Filipiak, M. J., Davis, C. P., Turquety, S., Wu, S. L., Park, R. J., Yantosca, R. M., and Jacob, D. J.: Convective outflow of South Asian pollution: A global CTM simulation compared with EOS MLS observations, Geophys Res Lett, 32, L14826, DOI 10.1029/2005gl022762, 2005.

Liou, K. N.: Cirrus clouds and climate in McGraw-Hill Yearbook of Science and Technology, McGraw-Hill Professional, New York, U.S.A., 2005.

Liu, X. H., and Penner, J. E.: Ice nucleation parameterization for global models, Meteorologische Zeitschrift, 14, 499-514, 10.1127/0941-2948/2005/0059, 2005.

Liu, X. H., Penner, J. E., and Wang, M. H.: Influence of anthropogenic sulfate and black carbon on upper tropospheric clouds in the NCAR CAM3 model coupled to the IMPACT global aerosol model, J Geophys Res-Atmos, 114, D03204, DOI 10.1029/2008jd010492, 2009.

Luebke, A. E., Afchine, A., Costa, A., Grooss, J. U., Meyer, J., Rolf, C., Spelten, N., Avallone, L. M., Baumgardner, D., and Kramer, M.: The origin of midlatitude ice clouds and the resulting influence on their microphysical properties, Atmos Chem Phys, 16, 5793-5809, 10.5194/acp-16-5793-2016, 2016.

Mace, G. G., Clothiaux, E. E., and Ackerman, T. P.: The composite characteristics of cirrus clouds: Bulk properties revealed by one year of continuous cloud radar data, J Climate, 14, 2185-2203, 10.1175/1520-0442(2001)014<2185:tccocc>2.0.co;2, 2001.

Mace, G. G., Benson, S., and Vernon, E.: Cirrus clouds and the large-scale atmospheric state: Relationships revealed by six years of ground-based data, J Climate, 19, 3257-3278, 10.1175/jcli3786.1, 2006.

Massie, S. T., Heymsfield, A., Schmitt, C., Muller, D., and Seifert, P.: Aerosol indirect effects as a function of cloud top pressure, J Geophys Res-Atmos, 112, D06202, DOI 10.1029/2006jd007383, 2007.

Muhlbauer, A., Ackerman, T. P., Comstock, J. M., Diskin, G. S., Evans, S. M., Lawson, R. P., and Marchand, R. T.: Impact of large-scale dynamics on the microphysical properties of midlatitude cirrus, J Geophys Res-Atmos, 119, 3976-3996, 10.1002/2013jd020035, 2014.

Murray, B. J., O'Sullivan, D., Atkinson, J. D., and Webb, M. E.: Ice nucleation by particles immersed in supercooled cloud droplets, Chem Soc Rev, 41, 6519-6554, 10.1039/c2cs35200a, 2012.

Ou, S. S. C., Liou, K. N., Wang, X. J., Hansell, R., Lefevre, R., and Cocks, S.: Satellite remote sensing of dust aerosol indirect effects on ice cloud formation, Appl Optics, 48, 633-642, 10.1364/Ao.48.000633, 2009.

Penner, J. E., Xu, L., and Wang, M. H.: Satellite methods underestimate indirect climate forcing by aerosols, P Natl Acad Sci USA, 108, 13404-13408, 10.1073/pnas.1018526108, 2011.

Platnick, S., King, M. D., and Meyer, K. G.: MODIS cloud optical properties: user guide for the collection 6 level-2 MOD06/MYD06 product and associated level-3 datasets: https://modis-images.gsfc.nasa.gov/_docs/C6MOD06OPUserGuide.pdf, 2015.

Pruppacher, H. R., and Klett, J. D.: Microphysics of Cloud and Precipitation, Springer, New York, U.S.A., 1997.

Remer, L. A., Kaufman, Y. J., Tanre, D., Mattoo, S., Chu, D. A., Martins, J. V., Li, R. R., Ichoku, C., Levy, R. C., Kleidman, R. G., Eck, T. F., Vermote, E., and Holben, B. N.: The MODIS aerosol algorithm, products, and validation, J Atmos Sci, 62, 947-973, Doi 10.1175/Jas3385.1, 2005.

Riihimaki, L. D., and McFarlane, S. A.: Frequency and morphology of tropical tropopause layer cirrus from CALIPSO observations: Are isolated cirrus different from those connected to deep convection?, J Geophys Res-Atmos, 115, 10.1029/2009jd013133, 2010.

Rosenfeld, D., Andreae, M. O., Asmi, A., Chin, M., de Leeuw, G., Donovan, D. P., Kahn, R., Kinne, S., Kivekas, N., Kulmala, M., Lau, W., Schmidt, K. S., Suni, T., Wagner, T., Wild, M., and Quaas, J.: Global observations of aerosol-cloud-precipitation-climate interactions, Rev Geophys, 52, 750-808, 10.1002/2013RG000441, 2014.

Seinfeld, J. H., Bretherton, C., Carslaw, K. S., Coe, H., DeMott, P. J., Dunlea, E. J., Feingold, G., Ghan, S., Guenther, A. B., Kahn, R., Kraucunas, I., Kreidenweis, S. M., Molina, M. J., Nenes, A., Penner, J. E., Prather, K. A., Ramanathan, V., Ramaswamy, V., Rasch, P. J., Ravishankara, A. R., Rosenfeld, D., Stephens, G., and Wood, R.: Improving our fundamental understanding of the role of aerosol-cloud interactions in the climate system, P Natl Acad Sci USA, 113, 5781-5790, 10.1073/pnas.1514043113, 2016.

Shi, X., and Liu, X.: Effect of cloud-scale vertical velocity on the contribution of homogeneous nucleation to cirrus formation and radiative forcing, Geophys Res Lett, 43, 6588-6595, 10.1002/2016GL069531, 2016.

Su, H., Jiang, J. H., Lu, X. H., Penner, J. E., Read, W. G., Massie, S., Schoeberl, M. R., Colarco, P., Livesey, N. J., and Santee, M. L.: Observed Increase of TTL Temperature and Water Vapor in Polluted Clouds over Asia, J Climate, 24, 2728-2736, 10.1175/2010JCLI3749.1, 2011.

Twomey, S.: Influence of pollution on shortwave albedo of clouds, J Atmos Sci, 34, 1149-1152, 10.1175/1520-0469(1977)034<1149:tiopot>2.0.co;2, 1977.

Waliser, D. E., Li, J. L. F., Woods, C. P., Austin, R. T., Bacmeister, J., Chern, J., Del Genio, A., Jiang, J. H., Kuang, Z. M., Meng, H., Minnis, P., Platnick, S., Rossow, W. B., Stephens, G. L., Sun-Mack, S., Tao, W. K., Tompkins, A. M., Vane, D. G., Walker, C., and Wu, D.: Cloud ice: A climate model challenge with signs and expectations of progress, J Geophys Res-Atmos, 114, D00a21, DOI 10.1029/2008jd010015, 2009.

Wang, F., Guo, J. P., Zhang, J. H., Huang, J. F., Min, M., Chen, T. M., Liu, H., Deng, M. J., and Li, X. W.: Multi-sensor quantification of aerosol-induced variability in warm clouds over eastern China, Atmos Environ, 113, 1-9, 10.1016/j.atmosenv.2015.04.063, 2015.

Wang, J. D., Zhao, B., Wang, S. X., Yang, F. M., Xing, J., Morawska, L., Ding, A. J., Kulmala, M., Kerminen, V. M., Kujansuu, J., Wang, Z. F., Ding, D. A., Zhang, X. Y., Wang, H. B., Tian, M., Petaja, T., Jiang, J. K., and Hao, J. M.: Particulate matter pollution over China and the effects of control policies, Sci Total Environ, 584, 426-447, 10.1016/j.scitotenv.2017.01.027, 2017.

Winker, D. M., Hunt, W. H., and McGill, M. J.: Initial performance assessment of CALIOP, Geophys Res Lett, 34, L19803, DOI 10.1029/2007gl030135, 2007.

Wylie, D. P., Menzel, W. P., Woolf, H. M., and Strabala, K. I.: 4 Years of Global Cirrus Cloud Statistics Using Hirs, J Climate, 7, 1972-1986, Doi 10.1175/1520-0442(1994)007<1972:Fyogcc>2.0.Co;2, 1994.

Wylie, D. P., Jackson, D. L., Menzel, W. P., and Bates, J. J.: Trends in global cloud cover in two decades of HIRS observations, J Climate, 18, 3021-3031, Doi 10.1175/Jcli3461.1, 2005.

Atmos. Chem. Phys. Discuss., https://doi.org/10.5194/acp-2017-548
Manuscript under review for journal Atmos. Chem. Phys.
Discussion started: 26 July 2017

Atmospheric Chemistry and Physics Discussions

Figures

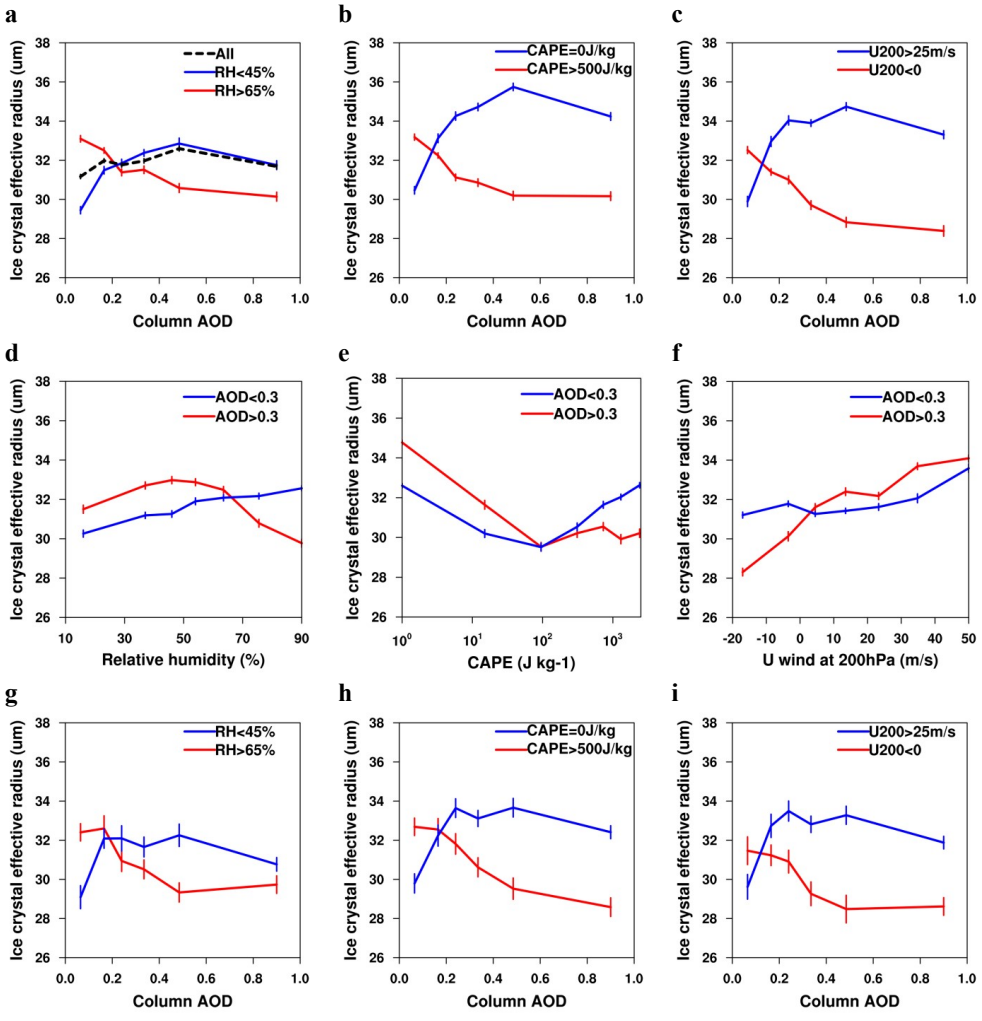

Figure 1. Influence of meteorological conditions on aerosol induced variability in ice crystal effective radius (R_{ei}) of ice clouds. (a-c) Changes in R_{ei} with AOD for different ranges of (a) RH averaged between 100 hPa and 440 hPa, (b) CAPE, and (c) U200. (d-f) Changes in R_{ei} with (d) RH, (e) CAPE, and (f) U200 for different ranges of AOD. (g-i) The same as (a-c) but for the profiles with dust aerosols only. The meteorological parameters and AOD are divided into 3 and 2 ranges containing similar numbers of data points, respectively; the curves for the medium meteorological range are not shown. The error bars denote the standard errors ($\sigma/\sqrt{N}$) of the bin average, where σ is the standard deviation and N is the sample number. The influences of other meteorological parameters are shown in Fig. S2.

Atmos. Chem. Phys. Discuss., https://doi.org/10.5194/acp-2017-548
Manuscript under review for journal Atmos. Chem. Phys.
Discussion started: 26 July 2017

Atmospheric Chemistry and Physics Discussions

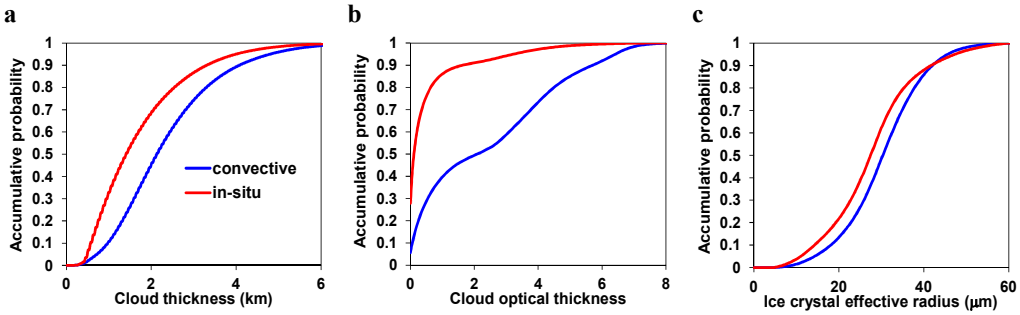

1 Figure 2. Accumulative probability distribution of the properties of two ice cloud types: (a)
2 cloud thickness, (b) cloud optical thickness, and (c) R_{ei}.
3

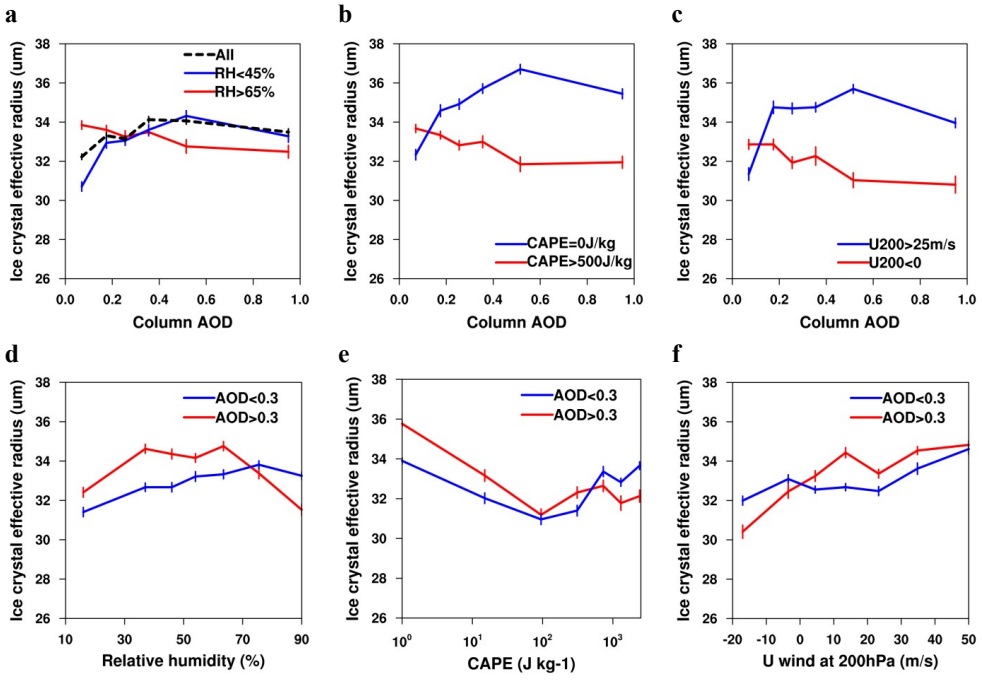

4 Figure 3. The same as Fig. 1a-f but for convective ice clouds.

Atmos. Chem. Phys. Discuss., https://doi.org/10.5194/acp-2017-548
Manuscript under review for journal Atmos. Chem. Phys.
Discussion started: 26 July 2017

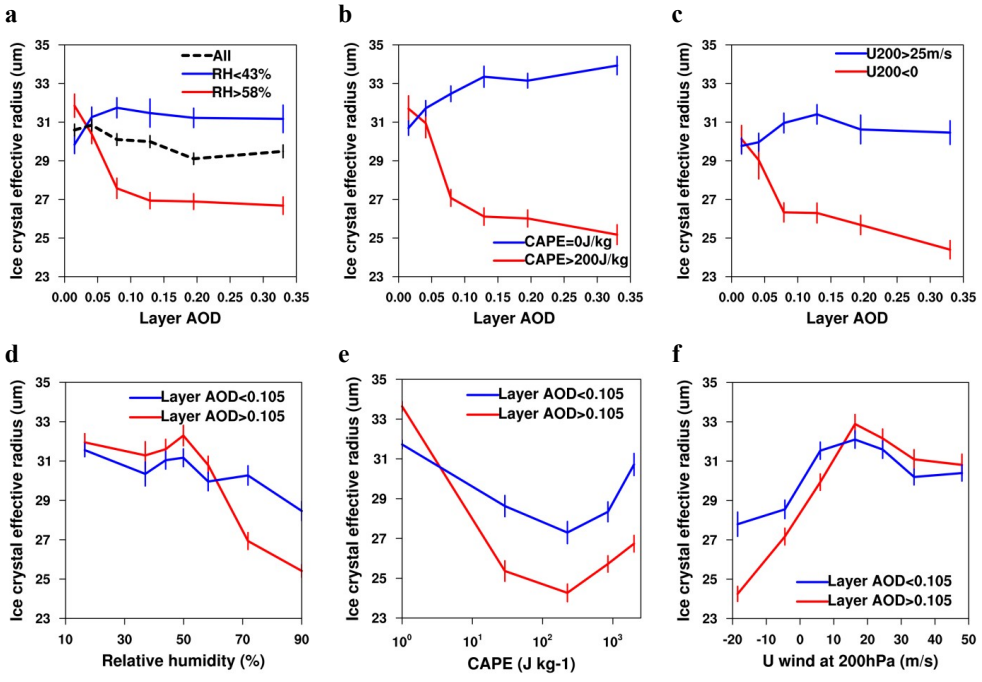

Figure 4. The same as Fig. 1a-f but for in-situ ice clouds. Note that we use AOD of the aerosol layers mixed with ice clouds rather than column AOD, since in-situ ice clouds are primarily affected by aerosols at the ice cloud height.

Atmos. Chem. Phys. Discuss., https://doi.org/10.5194/acp-2017-548
Manuscript under review for journal Atmos. Chem. Phys.
Discussion started: 26 July 2017

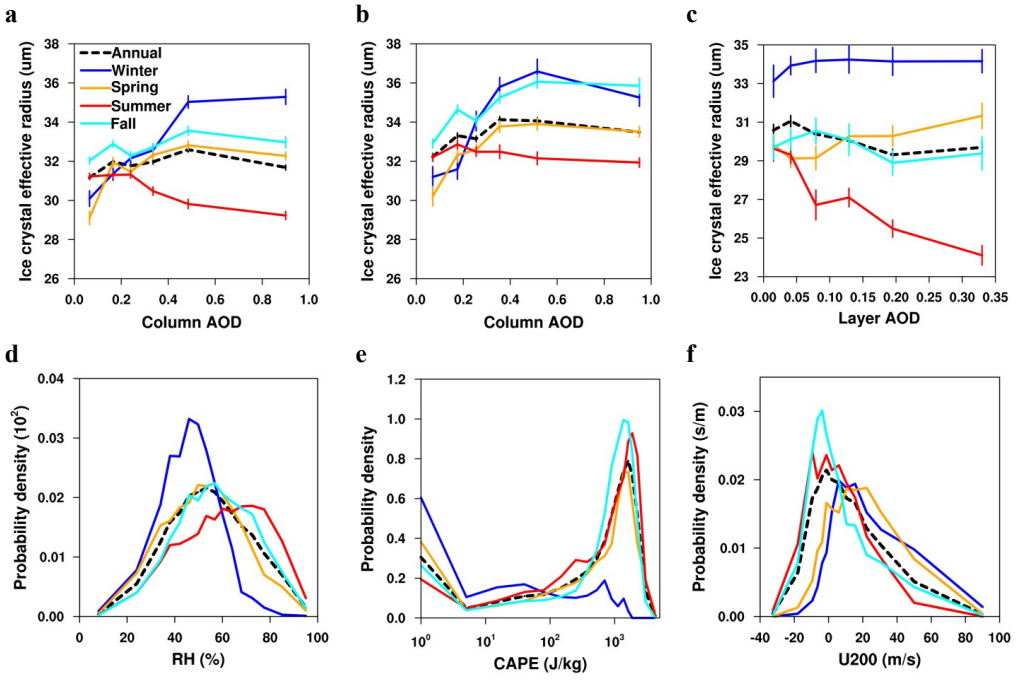

Figure 5. Changes in R_{ei} with AOD and the probability distribution of selected meteorological parameters as a function of season. (a-c) Changes in R_{ei} with AOD as a function of season for (a) all ice clouds, (b) convective ice clouds, and (c) in-situ ice clouds. (d-f) The probability distribution of (d) RH averaged between 100 hPa and 440 hPa, (e) CAPE, and (f) U200 as a function of season. Definitions of season are as follows: Winter – December, January, and February; Spring – March, April, and May; Summer – June, July, and August; Fall – September, October, and November. The definition of error bars is the same as in Fig. 1.

Atmos. Chem. Phys. Discuss., https://doi.org/10.5194/acp-2017-548
Manuscript under review for journal Atmos. Chem. Phys.
Discussion started: 26 July 2017

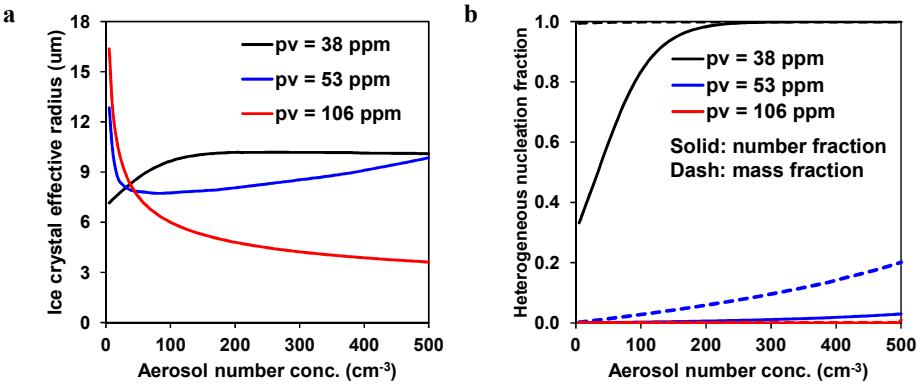

Figure 6. Simulated changes in (a) R_{ei} and (b) fraction of ice crystals produced by the heterogeneous nucleation as a function of the total aerosol number concentration. Simulations are conducted for three initial water vapor mass mixing ratios (pv), an indicator of available water amount for ice formation. The ratios of externally mixed dust (deposition INP), coated dust (immersion INP), and sulfate (not INP) are prescribed with values of 1.5:0.5:10000 in all experiments.